Charged-current neutrino-nucleus scattering off ^{95,97}Mo

E. Ydrefors* and J. Suhonen†
Department of Physics, University of Jyväskylä, Jyväskylä, Finland
(Received 7 December 2012; revised manuscript received 12 February 2013; published 11 March 2013)

Background: Reliable cross sections for the neutrino-nucleus scattering off relevant nuclei for supernova neutrinos are essential for various applications in neutrino physics and astrophysics (e.g., supernova mechanisms). Studies of the nuclear responses for the stable molybdenum isotopes are of great interest for the planned MOON (Mo Observatory of Neutrinos) experiment.
Purpose: The purpose of the present work is, thus, to perform a detailed study of the charged-current nuclear responses to supernova neutrinos for the stable odd molybdenum isotopes. A special effort will be devoted to discuss in detail the structures of the most relevant final states in the corresponding proton-odd nucleus.
Method: The cross sections are computed by using the well-established framework for studies of semileptonic processes in nuclei developed by Donnelly and Walecka. The nuclear wave functions of the initial and the final nuclear states are computed by using the microscopic quasiparticle-phonon model. The nuclear responses to supernova neutrinos are subsequently estimated by folding the cross sections with realistic energy profiles for the incoming neutrinos.
Results: We present results for the cross sections of the charged-current neutrino and antineutrino scatterings off ^{95}Mo and ^{97}Mo. Nuclear responses to supernova neutrinos (both nonoscillating and oscillating ones) are also given. The inclusion of neutrino oscillations enhances significantly the neutrino and antineutrino cross sections.
Conclusions: We have found that the most important transitions are the Gamow-Teller–like ones which are mediated by the 1^+ multipole. Furthermore, the three-quasiparticle degrees of freedom are essential in order to describe quantitatively the neutrino-nucleus scattering off odd open-shell nuclei.

DOI: 10.1103/PhysRevC.87.034314 PACS number(s): 25.30.Pt, 21.60.−n, 23.40.Bw, 27.60.+j

I. INTRODUCTION

During the last decades a tremendous progress has been achieved concerning experimental and theoretical studies of the neutrino and its properties. Outstanding examples include the observations of neutrinos from the Sun and supernovae, the verification of the nonzero mass of the neutrino and of neutrino oscillations. For a review on advances in neutrino physics, see, e.g., Ref. [1]. Recent experiments have also established that the third neutrino mixing angle, θ_{13}, has a relatively large value of $\sin^2\theta_{13} = 0.025$ [2].

However, several open questions still remain to be answered such as the Dirac-or-Majorana nature of the neutrino, normal-or-inverted neutrino-mass hierarchy and the absolute values of the neutrino masses. The studies of the neutrinoless double-beta ($0\nu\beta\beta$) decay of a selected set of even-even nuclei constitute a realistic way to determine the absolute mass spectrum of neutrinos [3,4]. An observation of the $0\nu\beta\beta$ decay would also provide direct evidence that the neutrino is a Majorana particle. One of the proposed candidates for these studies is ^{100}Mo. Hence, the investigations of nuclear structure for this nucleus and close-by nuclei are of great interest.

From the astrophysics side, weak interactions in nuclei play a crucial role both for the supernova dynamics and the nucleosynthesis of heavy elements [5,6]. The core-collapse supernovae constitute one of the proposed sites for the r-process [7]. Neutrino-induced nucleosynthesis in the supernova environment could also explain the abundances of some rare nuclei (see, e.g., Ref. [8]). It has been proposed [9] that the two nuclei ^{92}Nb and ^{98}Tc may have a neutrino-process origin. For the calculations of reaction rates of such processes reliable estimates of the neutrino-nucleus cross sections are needed.

A future detection of supernova neutrinos would be of great importance for both astrophysics and neutrino physics [10]. From the astrophysics point of view predictions by current supernova models could be tested and the distance to the supernova could be determined. Moreover, neutrino oscillations in dense matter could be studied.

Neutrinos from a future galactic supernova can be detected by charged-current and/or neutral-current neutrino-nucleus scatterings off nuclei [11]. Examples of current/planned possibilities for such measurements are the MOON (Mo Observatory of Neutrinos [12]), the HALO (Helium and Lead Observatory [13]), and the LAGUNA (Large Apparatus studying Grand Unification and Neutrino Astrophysics [14]). For the interpretation of the results from such measurements theoretical estimates of neutrino-nucleus cross sections are essential.

Computations of cross sections for the charged-current neutrino-nucleus scattering off medium-heavy odd nuclei are rarely found in the literature. The only published calculations are, to our knowledge, those of Ref. [15] for the neutrino reaction $^{127}\mathrm{I}(\nu_e, e^-)^{127}\mathrm{Xe}$, the ones of [16] for the charged-current scatterings off the stable even molybdenum isotopes, and the compilation of cross sections for r-process nuclei in Ref. [17]. In this paper we extend this short list of calculations and compute the cross sections for the charged-current neutrino

*e.ydrefors@gmail.com
†jouni.suhonen@phys.jyu.fi

and antineutrino scatterings off the stable odd molybdenum isotopes, ^{95}Mo and ^{97}Mo, for energies of the impinging neutrino which are relevant for supernova neutrinos. Theoretical estimates of the nuclear responses are subsequently computed by folding the cross sections with realistic energy profiles of the incoming neutrinos. Recent studies (see, e.g., Ref. [18]) have shown that so-called collective neutrino oscillations could play a significant play a significant role for supernova neutrinos. The effects of such neutrino flavor conversions are taken into account by the neutrino spectra which are adopted in this work. Furthermore, we discuss in detail the nuclear structure of the most important final nuclear states.

The foundation for the present calculations is the so-called Donnelly-Walecka formalism which was introduced in the seminal paper [19]. In Ref. [20] we developed an efficient method for the calculation of the required nuclear matrix elements which is based on the barycentric Lagrange interpolation [21]. This method is adopted also in this work. The initial and final nuclear states are constructed by using the microscopic quasiparticle-phonon model (MQPM [22]). In the MQPM, the three-quasiparticle degrees of freedom are incorporated by using as the basic building blocks the BCS (Bardeen-Cooper-Schrieffer) quasiparticles and QRPA (quasiparticle random-phase approximation [23]) phonons.

This paper is outlined as follows. First, in Sec. II we summarize the theoretical framework for the calculations of the charged-current neutrino-nucleus scattering cross sections. We present shortly also the basic formalism of the MQPM. Then, in Sec. III we discuss our results. Finally, in Sec. IV we draw the conclusions.

II. THEORY

A. Charged-current neutrino-nucleus scattering

In the present work the charged-current neutrino and antineutrino scatterings off a nucleus (A, Z) with mass number A and proton number Z are considered. We are interested in the neutrino reaction

$$(A, Z) + \nu_l \longrightarrow (A, Z+1) + l^-, \tag{1}$$

which proceed via the exchange of a W^- boson and the antineutrino reaction

$$(A, Z) + \bar{\nu}_l \longrightarrow (A, Z-1) + l^+, \tag{2}$$

where a W^+ boson is interchanged and $l = e, \mu, \tau$.

We use in the present paper conventions which are similar to whose of Ref. [24]. Hence, we define the four-momentum of the incoming neutrino as $k^\kappa = (E_\mathbf{k}, \mathbf{k})$ and that for the outgoing lepton as $k'^\kappa = (E_{\mathbf{k}'}, \mathbf{k}')$. The four momenta p^κ and p'^κ of the initial and final nuclear states are defined correspondingly. Furthermore, the four-momentum transfer for the (anti)neutrino scattering is given by $q_\kappa = k'_\kappa - k_\kappa = p_\kappa - p'_\kappa$.

For the low-energy neutrinos, such as, e.g., the supernova neutrinos, the transferred four-momentum is small compared to the mass of the exchanged particle, i.e., $Q^2 = -q_\kappa q^\kappa \ll M^2_{W^\pm}$. The matrix element of the effective Hamiltonian for the neutrino reaction (1) can then be written in the form

$$\langle f|H_{\rm eff}|i\rangle = \frac{G}{\sqrt{2}} \int d^3\mathbf{r} l_\kappa e^{-i\mathbf{q}\cdot\mathbf{r}} \langle f|\mathcal{J}^{(+),\kappa}(\mathbf{r})|i\rangle, \tag{3}$$

where $\mathcal{J}^{(+),\kappa}(\mathbf{r})$ denotes the hadron current and the lepton matrix element l_κ is defined as

$$l_\kappa = e^{i\mathbf{q}\cdot\mathbf{r}} \langle l|j^{(-)}_\kappa(\mathbf{r})|\nu\rangle, \tag{4}$$

where $j^{(-)}_\kappa(\mathbf{r})$ represents the lepton current. In Eq. (3) the coupling constant is $G = G_{\rm F}\cos\theta_{\rm C}$, where $G_{\rm F}$ is the Fermi constant and $\theta_{\rm C}$ denotes the Cabibbo angle. For the antineutrino-induced reaction (2) the currents $\mathcal{J}^{(+),\kappa}(\mathbf{r})$ and $j^{(-)}_\kappa(\mathbf{r})$ are to be replaced by their Hermitian conjugates, $\mathcal{J}^{(-),\kappa}(\mathbf{r})$ and $j^{(+)}_\kappa(\mathbf{r})$ respectively, in Eqs. (3) and (4).

At the origin ($\mathbf{r} = \mathbf{0}$) the one-nucleon matrix elements of the vector and axial-vector pieces of the current $\mathcal{J}^\kappa$ can be written in the forms

$$\begin{aligned} &{}_p\langle \mathbf{p}'\sigma'|J^{(+),V,\kappa}(0)|\mathbf{p}\sigma\rangle_n \\ &= \frac{\bar{u}(\mathbf{p}',\sigma')}{V}\left[F_1^{\rm CC}(Q^2)\gamma^\kappa - i\frac{F_2^{\rm CC}(Q^2)}{2m_N}\sigma^{\kappa\nu}q_\nu\right]u(\mathbf{p},\sigma), \end{aligned} \tag{5}$$

and

$$\begin{aligned} &{}_p\langle \mathbf{p}'\sigma'|J^{(+),A,\kappa}(0)|\mathbf{p}\sigma\rangle_n \\ &= \frac{\bar{u}(\mathbf{p}',\sigma')}{V}\left[F_A^{\rm CC}(Q^2)\gamma_5\gamma^\kappa + F_P^{\rm CC}(Q^2)\gamma_5 q^\kappa\right]u(\mathbf{p},\sigma), \end{aligned} \tag{6}$$

where $u(\mathbf{p},\sigma)$ is the Dirac spinor and for a free particle with three-momentum $\mathbf{p}$ and spin projection σ, and $\bar{u}(\mathbf{p},\sigma) = u^\dagger(\mathbf{p},\sigma)\gamma^0$ denotes the adjoint of $u(\mathbf{p},\sigma)$. Moreover, m_N represents the nucleon mass and the nucleon form factors $F^{\rm CC}_{1,2}(Q^2)$, $F^{\rm CC}_A(Q^2)$, and $F^{\rm CC}_P(Q^2)$ take into account the finite size of the nucleons. In the present computations we adopt the nucleon form factors of Ref. [16]. The axial-vector form factor $F^{\rm CC}_A(Q^2)$ is, thus, of a momentum-dipole form with the quenched static value $F^{\rm CC}_A(0) = -1.0$ for all multipoles J^π.

It is assumed that the final and initial nuclear states have well-defined angular momenta and parities. The double-differential cross section for the neutrino-nucleus scattering from an initial state i (with spin J_i) to a final state f (with spin J_f) is then given by

$$\begin{aligned} &\left(\frac{d^2\sigma_{i\to f}}{d\Omega dE_{\rm exc}}\right)_{\nu/\bar{\nu}} \\ &= \frac{G^2|\mathbf{k}'|E_{\mathbf{k}'}}{\pi(2J_i+1)}F(\pm Z_f, E_{\mathbf{k}'})\left(\sum_J \sigma^J_{\rm CL} + \sum_{J\geqslant 1}\sigma^J_T\right), \end{aligned} \tag{7}$$

where

$$\begin{aligned} \sigma^J_{\rm CL} &= (1 + a\cos\theta)|(J_f\|\mathcal{M}_J(q)\|J_i)|^2 \\ &\quad + (1 + a\cos\theta - 2b\sin^2\theta)|(J_f\|\mathcal{L}_J(q)\|J_i)|^2 \\ &\quad + \frac{E_{\rm exc}}{q}(1 + a\cos\theta + c) \\ &\quad \times 2{\rm Re}[(J_f\|\mathcal{L}_J(q)\|J_i)(J_f\|\mathcal{M}_J(q)\|J_i)^*], \end{aligned} \tag{8}$$

and

$$\sigma_T^J = (1 - a\cos\theta + b\sin^2\theta)\big[\big|\big(J_f\big\|\mathcal{T}_J^{\rm mag}(q)\big\|J_i\big)\big|^2 + \big|\big(J_f\big\|\mathcal{T}_J^{\rm el}(q)\big\|J_i\big)\big|^2\big] \mp \frac{E_{\mathbf{k}} + E_{\mathbf{k}'}}{q}(1 - a\cos\theta - c) \times 2{\rm Re}\big[\big(J_f\big\|\mathcal{T}_J^{\rm mag}(q)\big\|J_i\big)\big(J_f\big\|\mathcal{T}_J^{\rm el}(q)\big\|J_i\big)^*\big]. \quad (9)$$

In the expressions above the excitation energy $E_{\rm exc} = E_{\mathbf{p}'} - E_{\mathbf{p}}$ is computed with respect to the initial nuclear state and θ denotes the angle between the incoming and the outgoing leptons. In Eqs. (8) and (9) we have introduced the abbreviations

$$a = \sqrt{1 - (m_l/E_{\mathbf{k}'})^2}, \quad (10)$$

$$b = \frac{a^2 E_{\mathbf{k}} E_{\mathbf{k}'}}{q^2}, \quad (11)$$

and

$$c = \frac{m_l^2}{q E_{\mathbf{k}'}}, \quad (12)$$

where m_l denotes the mass of the outgoing lepton and the magnitude of the three-momentum transfer q is given by

$$q = |\mathbf{q}| = \sqrt{a^2 E_{\mathbf{k}'}^2 + E_{\mathbf{k}}^2 - 2a E_{\mathbf{k}} E_{\mathbf{k}'}\cos\theta}. \quad (13)$$

Furthermore, in Eq. (9) the minus sign is used for neutrinos and the plus sign for antineutrinos. The nuclear dependence of the cross sections is contained in the nuclear matrix elements of the multipole operators $\mathcal{M}_{JM}(q)$, $\mathcal{L}_{JM}(q)$, $\mathcal{T}_{JM}^{\rm el}(q)$, and $\mathcal{T}_{JM}^{\rm mag}(q)$. For the definitions of these operators, see, e.g., Ref. [25]. The function $F(\pm Z_f, E_{\mathbf{k}'})$ in Eq. (7) takes into account the distortion of the final lepton wave function by the Coulomb field of the final nucleus. The "+" sign is adopted for leptons and the "−" sign for antileptons. We adopt in this work the treatment of F introduced in Ref. [26]. For more details, see, e.g., Refs. [16,27].

B. MQPM

In this work the wave functions of the initial and final nuclear states are computed by using the microscopic quasiparticle-phonon model (MQPM). Therefore, in this section we summarize the basic concepts of the MQPM. For a more comprehensive treatment we refer to [22].

The basic building blocks in the MQPM are the BCS quasiparticles and the QRPA (quasiparticle random-phase approximation) phonons. The quasiparticles are first defined via the Bogoliubov-Valatin transformation as

$$a_\beta^\dagger = u_b c_\beta^\dagger + v_b \tilde{c}_\beta, \quad \tilde{a}_\beta = u_b \tilde{c}_\beta - v_b c_\beta^\dagger, \quad (14)$$

where the index b includes the single-particle quantum numbers n_b, l_b and j_b, and $\beta = (b, m_\beta)$ where m_β is the magnetic quantum number. In Eq. (14) $c_\beta^\dagger$ is the particle creation operator and $\tilde{c}_\beta = (-1)^{j_b + m_\beta} c_{-\beta}$, denotes the time-reversed particle annihilation operator where $-\beta = (b, -m_\beta)$. Here the occupation amplitudes u_b and v_b are obtained by solving the BCS equations of motion (see, e.g., Ref. [28]).

The QRPA phonons are then formed by coupling two-quasiparticle configurations to good angular momentum J_ω and parity π_ω. Consequently, the QRPA creation operator for an excitation $\omega = (J_\omega, \pi_\omega, k_\omega)$ is given by

$$Q_\omega^\dagger = \sum_{b \leqslant b'} \sigma_{bb'}^{-1}\big(X_{bb'}^\omega [a_b^\dagger a_{b'}^\dagger]_{J_\omega M_\omega} + Y_{bb'}^\omega [\tilde{a}_b \tilde{a}_{b'}]_{J_\omega M_\omega}\big), \quad (15)$$

where $\sigma_{bb'} = \sqrt{1 + \delta_{bb'}}$ and the sum runs over all proton-proton and neutron-neutron configurations, in the chosen valence space, so that none of them are counted twice. Here k_ω enumerates the phonons with the same angular momentum J_ω and parity π_ω.

In the MQPM a state with angular momentum j and projection m in an odd-A nucleus is then created by using the operator

$$\Gamma_k^\dagger(jm) = \sum_n D_n^k a_{njm}^\dagger + \sum_{b\omega} D_{b\omega}^k [a_b^\dagger Q_\omega^\dagger]_{jm}. \quad (16)$$

The MQPM amplitudes D_n^k and $D_{b\omega}^k$ are solved from the MQPM equations of motion [22]. While solving these equations special care has to be taken to handle the overcompleteness and nonorthogonality of the quasiparticle-phonon basis. The MQPM states with one dominant amplitude D_n^k are called one-quasiparticle–like and the states with one, few or many important amplitudes $D_{b\omega}^k$ are called three-quasiparticle–like ones.

III. RESULTS AND DISCUSSION

In this section we employ the formalism presented in Sec. II to compute the cross sections for the neutrino and antineutrino scatterings off ^{95}Mo and ^{97}Mo. In the present calculations we use for the initial nuclear states, i.e., the ground states of ^{95}Mo and ^{97}Mo, respectively, the nuclear wave functions computed in [20]. The final nuclear states in ^{95}Tc, ^{97}Tc, ^{95}Nb, or ^{97}Nb are calculated similarly. Thus, the single-particle energies are computed from the Coulomb-corrected Woods-Saxon potential with the parametrization of Ref. [29] and the Bonn one-boson-exchange potential [30] is used as the two-body interaction in both the BCS and the QRPA calculations. Furthermore, we adopt the large quasiparticle-phonon basis of [20] and the parameters of the BCS and the QRPA calculations are adjusted according to Ref. [31].

We subsequently compute the double-differential cross sections (7) for each final state, scattering angle θ and energy $E_{\mathbf{k}}$ of the incoming (anti)neutrino. The total cross section, $\sigma(E_{\mathbf{k}})$, as a function of the neutrino energy, is then calculated by summing up the contributions from all the final states and subsequently integrating (numerically) over the angle θ.

Table I shows the cross sections for the neutrino and antineutrino scatterings off ^{95}Mo and ^{97}Mo as functions of the energy of the impinging particle. It is seen in the table that both the neutrino and antineutrino cross sections increase significantly with the neutrino energy. The cross sections for the neutrinos are also substantially larger than the ones for antineutrinos. Furthermore, we can conclude that the neutrino

TABLE I. Cross sections for the charged-current neutrino and antineutrino scatterings off ^{95,97}Mo in units of 10^{-42}cm^2 as functions of the energy of the incoming neutrino. Exponents are given in parenthesis.

Energy/MeV	^{95}Mo + ν_e	^{95}Mo + $\bar{\nu}_e$	^{97}Mo + ν_e	^{97}Mo + $\bar{\nu}_e$
5.0	2.06 (−3)	1.64 (−3)	2.04 (−2)	5.28 (−5)
10.0	7.55 (−1)	1.87 (−1)	1.54 (0)	1.26 (−1)
15.0	6.04 (0)	6.44 (−1)	9.79 (0)	5.14 (−1)
20.0	1.99 (1)	1.41 (0)	2.82 (1)	1.19 (0)
25.0	4.27 (1)	2.53 (0)	5.59 (1)	2.19 (0)
30.0	7.18 (1)	4.07 (0)	8.88 (1)	3.58 (0)
40.0	1.42 (2)	8.56 (0)	1.65 (2)	7.64 (0)
50.0	2.36 (2)	1.58 (1)	2.64 (2)	1.43 (1)
60.0	3.32 (2)	2.70 (1)	3.65 (2)	2.45 (1)
70.0	4.26 (2)	4.06 (1)	4.63 (2)	3.72 (1)
80.0	5.12 (2)	5.49 (1)	5.52 (2)	5.09 (1)

cross sections increase with the neutron number and that for the antineutrinos the trend is the opposite.

One important quantity from the experimental point of view is the averaged cross section, $\langle\sigma\rangle$, which is obtained by folding the cross section with an appropriate energy profile for the incoming neutrinos. The energies of supernova neutrinos can reasonably well be described by a two-parameter Fermi-Dirac distribution

$$F_{\rm FD}(E_{\mathbf{k}}) = \frac{1}{F_2(\alpha_\nu)T_\nu}\frac{(E_{\mathbf{k}}/T_\nu)^2}{1+\exp(E_{\mathbf{k}}/T_\nu-\alpha_\nu)}, \tag{17}$$

where T_ν represents the effective neutrino temperature and α_ν is the pinching parameter. For a given value of α_ν the temperature T_ν can be computed from the average neutrino energy $\langle E_\nu\rangle$ by using the relation

$$\langle E_\nu\rangle/T_\nu = \frac{F_3(\alpha_\nu)}{F_2(\alpha_\nu)}, \tag{18}$$

where

$$F_k(\alpha_\nu) = \int \frac{x^k dx}{1+\exp(x-\alpha_\nu)}. \tag{19}$$

Because of the large muon and tau rest masses only electron neutrinos (electron antineutrinos) from supernovae can be detected by charged-current neutrino-nucleus scattering. Neutrinos can, however, undergo flavor conversions due to interactions with the matter of the star. According to recent studies (see, e.g., Ref. [18]) collective neutrino oscillations caused by neutrino-neutrino interactions are also important. It is usually assumed that the neutrino-energy spectra of muon and tau neutrinos are the same. The energy profiles

TABLE II. Averaged cross sections for the charged-current neutrino and antineutrino scatterings off ^{95}Mo and ^{97}Mo in units of 10^{-41} cm^2 computed with the neutrino parameters shown in Table III.

Nucleus	ν_e	$\nu_{ex}^{\rm NH}$	$\nu_{ex}^{\rm IH}$	$\bar{\nu}_e$	$\bar{\nu}_{ex}^{\rm NH}$	$\bar{\nu}_{ex}^{\rm IH}$
^{95}Mo	5.12	20.8	20.8	0.723	1.44	0.932
^{97}Mo	7.52	26.7	26.7	0.598	1.24	0.784

TABLE III. Adopted values of the average neutrino energy $\langle E_\nu\rangle$ and the pinching parameter α_ν for the various neutrino flavors. The corresponding neutrino temperatures T_ν are also given.

Flavor	$\langle E_\nu\rangle$/MeV	α_ν	T_ν/MeV
ν_e	11.5	3.0	2.88
$\bar{\nu}_e$	13.6	3.0	3.41
ν_μ, ν_τ, $\bar{\nu}_\mu$, $\bar{\nu}_\tau$	16.3	0.0	5.17

for electron neutrinos and electron antineutrinos which reach an Earth-bound detector can then be written in the forms

$$F_{\nu_e}(E_{\mathbf{k}}) = p(E_{\mathbf{k}})F^0_{\nu_e}(E_{\mathbf{k}}) + (1-p(E_{\mathbf{k}}))F^0_{\nu_x}(E_{\mathbf{k}}), \tag{20}$$

and

$$F_{\bar{\nu}_e}(E_{\mathbf{k}}) = \bar{p}(E_{\mathbf{k}})F^0_{\bar{\nu}_e}(E_{\mathbf{k}}) + (1-\bar{p}(E_{\mathbf{k}}))F^0_{\bar{\nu}_x}(E_{\mathbf{k}}), \tag{21}$$

where p ($\bar{p}$) denotes the survival probability of electron neutrinos (electron antineutrinos). Here $F^0_{\nu_e}(E_{\mathbf{k}})$ ($F^0_{\bar{\nu}_e}(E_{\mathbf{k}})$) and $F^0_{\nu_x}(E_{\mathbf{k}})$ ($F^0_{\bar{\nu}_x}(E_{\mathbf{k}})$) are the initial energy profiles of electron neutrinos (electron antineutrinos) and nonelectron neutrinos (nonelectron antineutrinos), respectively. Guided by Refs. [10,32] we use for the survival probability $p(E_{\mathbf{k}})$ ($\bar{p}(E_{\mathbf{k}})$) of electron neutrinos (electron antineutrinos) in the case of normal mass hierarchy the prescriptions

$$p(E_{\mathbf{k}}) = 0, \tag{22}$$

and

$$\bar{p}(E_{\mathbf{k}}) = \begin{cases} 1; & E_{\mathbf{k}} < \bar{E}_s, \\ 0; & E_{\mathbf{k}} > \bar{E}_s, \end{cases} \tag{23}$$

with the split energy $\bar{E}_s = 18.0$ MeV [32]. Similarly, for the inverted mass hierarchy we adopt the survival probabilities

$$p(E_{\mathbf{k}}) = \begin{cases} \sin^2\theta_{12}; & E_{\mathbf{k}} < E_s, \\ 0; & E_{\mathbf{k}} > E_s, \end{cases} \tag{24}$$

and

$$\bar{p}(E_{\mathbf{k}}) = \cos^2\theta_{12}, \tag{25}$$

for electron neutrinos and electron antineutrinos, respectively. Here we adopt the value $E_s = 7$ MeV [33]. Equations (20) and (21) are valid for general energy profiles of the supernova

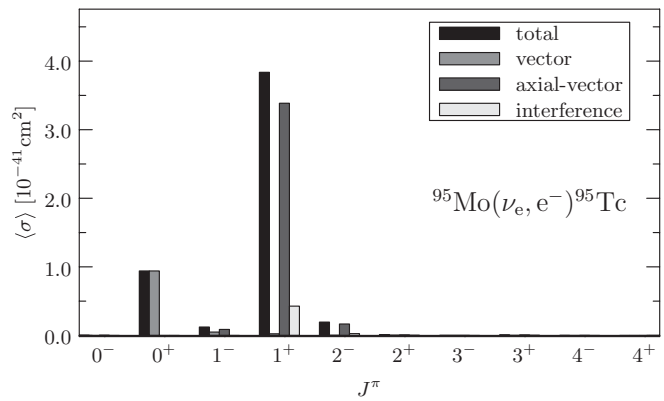

FIG. 1. Contributions from the prominent multipole channels to the charged-current neutrino scattering off ^{95}Mo.

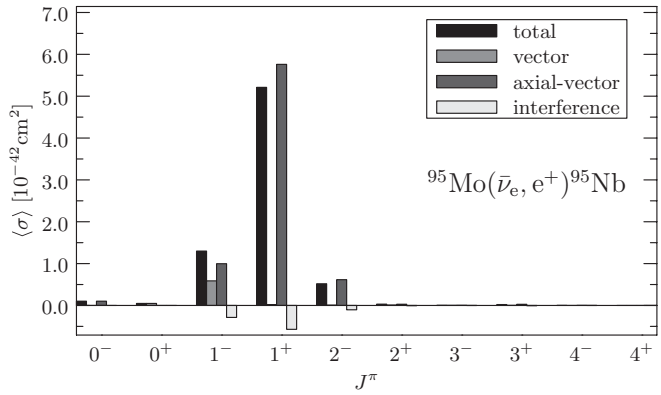

FIG. 2. Contributions from the prominent multipole channels to the charged-current antineutrino scattering off ^{95}Mo.

neutrinos. However, in the present calculations we adopt energy distributions of the Fermi-Dirac type (17).

In Table II we show the computed averaged cross sections for the charged-current neutrino and antineutrino scatterings off the odd stable Mo nuclei. In the table ν_e ($\bar{\nu}_e$) denote nonoscillating neutrinos (antineutrinos). Moreover, $\nu_{ex}^{\rm NH}$ ($\bar{\nu}_{ex}^{\rm NH}$) and $\nu_{ex}^{\rm IH}$ ($\bar{\nu}_{ex}^{\rm IH}$) represent oscillating neutrinos (antineutrinos) in the cases of normal (NH) and inverted (IH) mass hierarchy, respectively. The results in the table correspond to the neutrino parameters of Table III. However, averaged cross sections for other neutrino profiles can be easily computed by using the cross sections which are tabulated in Table I. In the computations the corresponding neutrino temperatures T_ν are computed from the average neutrino temperatures $\langle E_\nu\rangle$ of Table III by using Eq. (18). It is seen in Table II that the nuclear responses increase significantly when neutrino conversions are included in the calculations. Furthermore, the cross sections for the neutrino scattering are practically independent of the neutrino-mass hierarchy. Contrary to this, for the antineutrinos the cross sections are significantly larger for the normal mass hierarchy than for the inverted mass hierarchy.

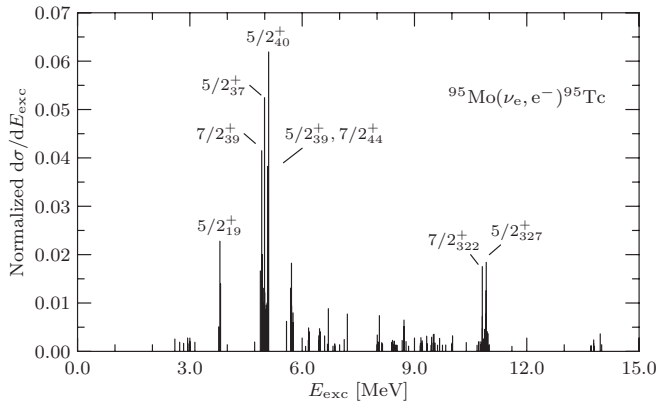

FIG. 3. Differential cross sections for the charged-current neutrino scattering off ^{95}Mo to final states in ^{95}Tc. In the figure the states are labeled j_k^π where the number k enumerates states with the same angular momentum j and parity π in order of increasing excitation energy $E_{\rm exc}$.

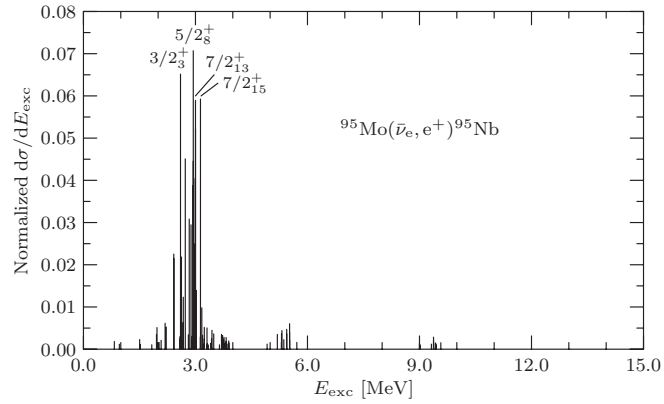

FIG. 4. Differential cross sections for the charged-current antineutrino scattering off ^{95}Mo to final states in ^{95}Nb. In the figure the states are labeled j_k^π where the number k enumerates states with the same angular momentum j and parity π in order of increasing excitation energy $E_{\rm exc}$.

In Fig. 1 the contributions coming from the most important multipole channels of Eq. (7) to the averaged cross sections for the neutrino scattering off ^{95}Mo are shown. The results for the antineutrino scattering are similarly displayed in Fig. 2. In the figures we also show for each multipole J^π the contributions coming from the vector and axial-vector parts of the nuclear current. We can conclude from Figs. 1 and 2 that for both the neutrino and antineutrino reactions the 1^+ multipole transitions dominate the cross sections. Furthermore, the most important transitions are of the axial-vector type. Fermi-like transitions, mediated by the 0^+ multipole, are also important for the neutrino-nucleus scattering. These general conclusions, i.e., that the neutrino cross sections are dominated by Gamow-Teller–like and Fermi-like transitions, are also in agreement with, e.g., the calculations performed for ^{56}Fe in Ref. [34]. However, for the antineutrino reaction (2) the contribution from the 0^+ multipole is largely suppressed and consequently 1^- and 2^- spin-dipole type of transitions become more important.

Moreover, in Fig. 3 (Fig. 4) we show the differential cross sections for the charged-current (anti)neutrino scattering leading to final states in ^{95}Tc (^{95}Nb). Similarly, the results for the neutrino and antineutrino scatterings off ^{97}Mo are

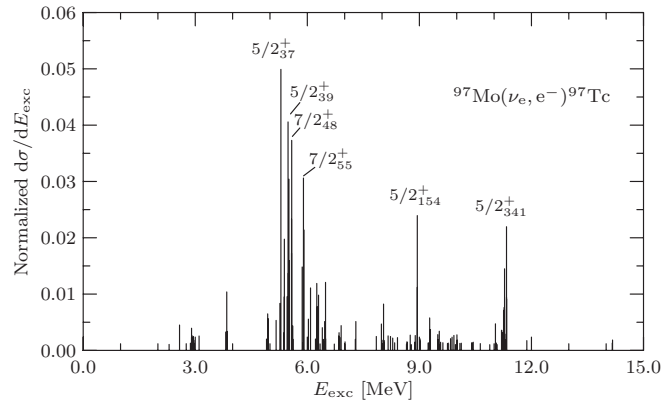

FIG. 5. Same as Fig. 3 but for the neutrino scattering off ^{97}Mo.

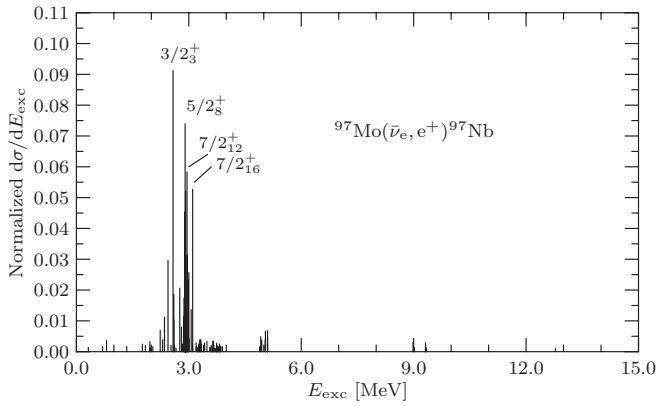

FIG. 6. Same as Fig. 4 but for the antineutrino scattering off ^{97}Mo.

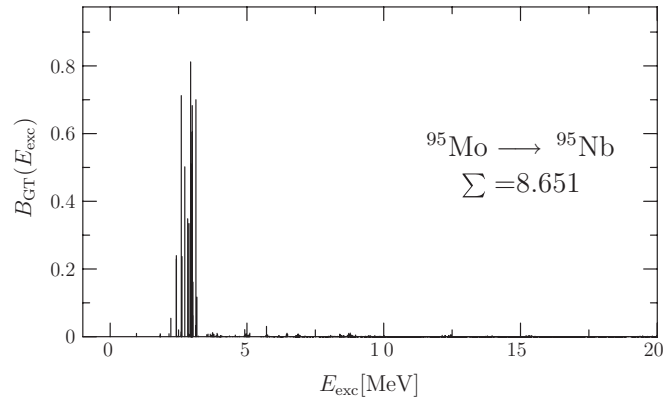

FIG. 8. β^+ strength for transitions to final states in ^{95}Nb.

displayed in Figs. 5 and 6. It is seen in the figures that the dominant states are $3/2^+$, $5/2^+$, and $7/2^+$ final states. This is in agreement with the fact that transitions mediated by the 1^+ multipole are the most important ones as discussed above. However, the final nuclear states in the neutrino-induced reactions are spread over a large span of excitation energies. On the contrary, for the antineutrino scattering the most prominent final states have excitation energies around $E_{exc} \approx 3.0$ MeV.

For small energies of the incoming neutrino or antineutrino the 1^+ transitions are mediated by Gamow-Teller–like operators $j_0(qr)\boldsymbol{\sigma}\tau_\pm$. In the limit when the magnitude of the three-momentum transfer q approaches zero the aforementioned operators reduce to the usual Gamow-Teller operators $\boldsymbol{\sigma}\tau_\pm$. Consequently, in Fig. 7 are shown the strength functions for the Gamow-Teller β^- type of transitions from the $5/2^+$ ground state of ^{95}Mo to $3/2^+$, $5/2^+$, and $7/2^+$ final states in ^{95}Tc. The results for the β^+ transitions to final states in ^{95}Nb are similarly presented in Fig. 8. Unfortunately, no experimental strength functions are available for comparison. As can be seen in the figures the total β^- strength is much larger than the β^+ strength, which is in agreement with results for heavy even-even nuclei. It is well known that for the even-even nuclei the difference between the total Gamow-Teller β^- and β^+ strengths satisfy the Ikeda sum rule [35], which for the reference nucleus ^{94}Mo would read $3(N-Z) = 30$. In the present calculation for the odd-mass ^{95}Mo the corresponding difference in the total strengths reads 24.7 and is thus somewhat smaller than the Ikeda sum rule for the even-even reference nucleus. The difference stems from the fact that in the presently adopted formalism the phonons stem from the QRPA and not from the *pn*QRPA which automatically satisfies the Ikeda sum rule for the computed Gamow-Teller strengths [28]. An improvement in this respect can be achieved by taking the phonons from the *pn*QRPA and coupling them with the quasiparticles as was done in [36]. However, the formalism of [36] lacks some important three-quasiparticle contributions that can contribute to collective excitations. An other source of missing the Ikeda sum rule in the present calculations is that for the sake of the CPU usage we have not employed the full set of QRPA phonons in the computations, but rather a truncated subset. This may reduce the β^- strength at high excitation energies, beyond 15 MeV. As implied by Eq. (7) this missing strength at high energies would not influence notably the charged-current neutrino scattering due to the small momentum and kinetic energy of the final-state lepton.

Furthermore, in Fig. 9 the Gamow-Teller strength functions are decomposed into the contributions coming from the possible $3/2^+$, $5/2^+$, and $7/2^+$ final states. As is seen in the figure the transitions to $5/2^+$ final states are the most important for the β^- strength. Instead, for the β^+ mode the transitions to $7/2^+$ states are the most prominent. The differences between

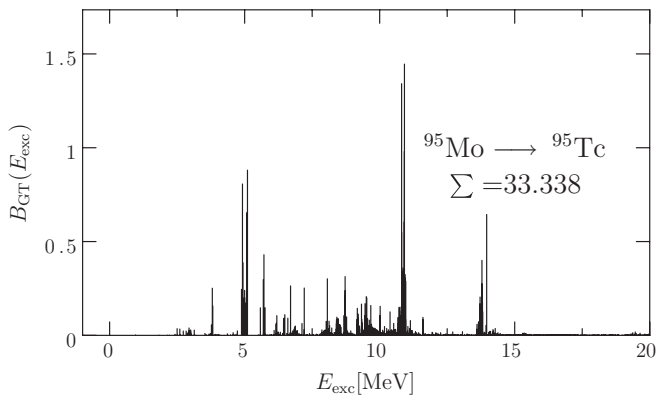

FIG. 7. β^- strength for transitions to final states in ^{95}Tc.

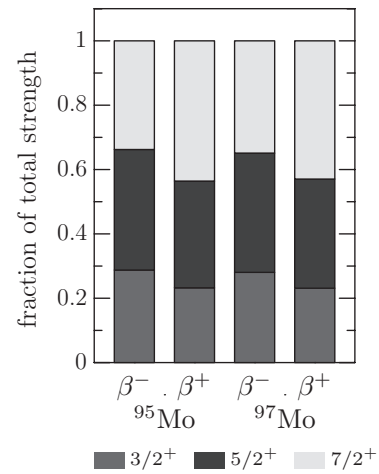

FIG. 9. Contributions to the β^- and β^+ total strengths, respectively, for ^{95}Mo and ^{97}Mo.

TABLE IV. MQPM amplitudes X^f for some important states in ^{95}Tc.

State	Conf.	X^f
$5/2^+_{40}$	$\pi 1d_{5/2} \otimes 2^+_1$	−0.681
	$\pi 0g_{9/2} \otimes 2^+_{15}$	−0.374
	$\pi 0g_{9/2} \otimes 3^+_8$	−0.319
	$\pi 1d_{5/2} \otimes 2^+_2$	0.307
	$\pi 1d_{5/2}$	−0.167
	$\pi 1d_{5/2} \otimes 2^+_3$	−0.156
	$\pi 0g_{9/2} \otimes 2^+_{17}$	0.117
	$\pi 0g_{9/2} \otimes 2^+_{14}$	−0.104
$5/2^+_{37}$	$\pi 0g_{9/2} \otimes 4^+_{10}$	−0.747
	$\pi 0g_{9/2} \otimes 6^+_4$	0.596
	$\pi 0g_{9/2} \otimes 4^+_8$	0.141
	$\pi 1d_{5/2}$	0.046
$7/2^+_{39}$	$\pi 0g_{9/2} \otimes 6^+_4$	0.936
	$\pi 0g_{9/2} \otimes 2^+_{15}$	0.126
	$\pi 0g_{7/2}$	−0.117
	$\pi 0g_{9/2} \otimes 6^+_2$	0.116
	$\pi 1f_{5/2} \otimes 2^+_1$	0.116
$5/2^+_{39}$	$\pi 0g_{9/2} \otimes 5^+_3$	0.991
	$\pi 0g_{9/2} \otimes 3^+_8$	−0.113
$7/2^+_{44}$	$\pi 0g_{9/2} \otimes 5^+_3$	0.995
$5/2^+_{19}$	$\pi 1d_{5/2}$	−0.659
	$\pi 0g_{9/2} \otimes 2^+_8$	0.583
	$\pi 0g_{9/2} \otimes 2^+_7$	−0.275
	$\pi 0g_{9/2} \otimes 2^+_{10}$	−0.191
	$\pi 0g_{9/2} \otimes 2^+_9$	−0.124
$7/2^+_{322}$	$\pi 0g_{7/2} \otimes 6^+_4$	−0.795
	$\pi 1d_{3/2} \otimes 4^+_6$	0.393
	$\pi 1d_{5/2} \otimes 1^+_6$	0.221
	$\pi 0f_{5/2} \otimes 5^-_{15}$	0.150
	$\pi 0f_{5/2} \otimes 3^-_{20}$	0.115
$5/2^+_{327}$	$\pi 0g_{7/2} \otimes 5^+_3$	0.581
	$\pi 1d_{5/2} \otimes 1^+_6$	−0.442
	$\pi 0g_{7/2} \otimes 3^+_8$	−0.236
	$\pi 0f_{5/2} \otimes 4^-_{19}$	−0.229
	$\pi 2s_{1/2} \otimes 2^+_{15}$	0.167
	$\pi 0f_{5/2} \otimes 4^-_{20}$	−0.142
	$\pi 1p_{3/2} \otimes 4^-_{19}$	−0.136
	$\pi 1p_{3/2} \otimes 4^-_{18}$	−0.134
	$\pi 0g_{7/2} \otimes 6^+_4$	−0.100

the three groups of transitions are, however, quite small and the conclusions could be affected by uncertainties, e.g., in the nuclear structure.

More information about the prominent final states in Figs. 3–6 can be obtained by studying the MQPM amplitudes D^k_n and $D^k_{b\omega}$ of Eq. (16). Therefore, we tabulate in Table IV (Table V) the MQPM amplitudes for some of the prominent states for the charged-current (anti)neutrino scattering off ^{95}Mo, see also Figs. 3 and 4. The corresponding results for ^{97}Mo are shown in Tables VI and VII, respectively. The $5/2^+$ ground states of ^{95}Mo and ^{97}Mo can to a good approximation be considered as $\nu 1d_{5/2}$ one-quasiparticle states. As is seen in Tables IV and VI the neutrino scatterings to states in

TABLE V. MQPM amplitudes X^f for some important states in ^{95}Nb.

State	Conf.	X^f
$5/2^+_8$	$\pi 0g_{9/2} \otimes 5^+_1$	−1.000
$3/2^+_3$	$\pi 0g_{9/2} \otimes 4^+_2$	−0.625
	$\pi 0g_{9/2} \otimes 6^+_1$	−0.608
	$\pi 0g_{9/2} \otimes 6^+_2$	−0.357
	$\pi 0g_{9/2} \otimes 4^+_3$	−0.307
$7/2^+_{13}$	$\pi 0g_{9/2} \otimes 4^+_4$	−0.954
	$\pi 0g_{9/2} \otimes 4^+_3$	0.264
	$\pi 0g_{9/2} \otimes 2^+_4$	−0.102
$7/2^+_{15}$	$\pi 0g_{9/2} \otimes 2^+_5$	0.990

^{95}Tc and ^{97}Tc are dominated by single-particle transitions of the forms $\nu 1d_{5/2} \longrightarrow \pi 1d_{5/2}$, $\nu 1d_{5/2} \longrightarrow \pi 1d_{5/2} \otimes \omega$, $\nu 1d_{5/2} \longrightarrow \pi 1d_{3/2} \otimes \omega$, and $\nu 1d_{5/2} \longrightarrow \pi 0g_{9/2} \otimes \omega$ for various QRPA phonons ω. Interestingly, for the scattering to ^{95}Tc the $7/2^+_{39}$ state in Table IV has a rather large amplitude for the $\pi 0g_{7/2}$ one-quasiparticle configuration. But the nuclear matrix element for the l-forbidden $\nu 1d_{5/2} \longrightarrow \pi 0g_{7/2}$ transition vanishes to lowest order in the three-momentum transfer q so that this component of the final state does not play a role in the transition strength. Furthermore, we can conclude from Tables V and VII that the most prominent single-particle

TABLE VI. MQPM amplitudes X^f for some important states in ^{97}Tc.

State	Conf.	X^f
$5/2^+_{37}$	$\pi 0g_{9/2} \otimes 2^+_{15}$	0.863
	$\pi 1d_{5/2} \otimes 2^+_1$	0.225
	$\pi 1p_{1/2} \otimes 3^-_3$	0.134
	$\pi 1d_{5/2} \otimes 2^+_2$	−0.132
	$\pi 0g_{9/2} \otimes 2^+_{11}$	−0.129
	$\pi 0f_{5/2} \otimes 5^-_4$	0.105
	$\pi 0g_{9/2} \otimes 2^+_{16}$	−0.104
	$\pi 1d_{5/2}$	−0.101
$5/2^+_{39}$	$\pi 0g_{9/2} \otimes 4^+_{10}$	0.616
	$\pi 0g_{9/2} \otimes 6^+_4$	0.556
	$\pi 1p_{3/2} \otimes 3^-_3$	−0.375
	$\pi 0g_{9/2} \otimes 3^+_8$	−0.148
	$\pi 1p_{3/2} \otimes 3^-_1$	−0.123
$7/2^+_{48}$	$\pi 0g_{9/2} \otimes 5^+_3$	−0.862
	$\pi 0g_{7/2}$	−0.353
	$\pi 0g_{9/2} \otimes 6^+_4$	0.225
	$\pi 0f_{5/2} \otimes 3^-_3$	−0.123
$7/2^+_{55}$	$\pi 1d_{5/2} \otimes 4^+_1$	−0.842
	$\pi 0g_{9/2} \otimes 6^+_5$	−0.350
	$\pi 1p_{3/2} \otimes 4^-_4$	−0.215
$5/2^+_{154}$	$\pi 1d_{3/2} \otimes 4^+_1$	0.941
	$\pi 1d_{3/2} \otimes 4^+_4$	0.102
$5/2^+_{341}$	$\pi 0g_{7/2} \otimes 5^+_3$	0.996
	$\pi 1d_{5/2} \otimes 1^+_6$	−0.058

TABLE VII. MQPM amplitudes X^f for some important states in ^{97}Nb.

State	Conf.	X^f
$5/2^+_8$	$\pi 0g_{9/2} \otimes 5^+_1$	1.000
$3/2^+_3$	$\pi 0g_{9/2} \otimes 6^+_1$	−0.763
	$\pi 0g_{9/2} \otimes 4^+_2$	0.437
	$\pi 0g_{9/2} \otimes 6^+_2$	0.382
	$\pi 0g_{9/2} \otimes 4^+_3$	0.176
	$\pi 0g_{9/2} \otimes 4^+_4$	0.161
$7/2^+_{13}$	$\pi 0g_{9/2} \otimes 3^+_3$	−0.968
	$\pi 0g_{9/2} \otimes 1^+_1$	0.289
	$\pi 0g_{9/2} \otimes 2^+_4$	0.205
	$\pi 0g_{9/2} \otimes 1^+_2$	−0.122
$7/2^+_{16}$	$\pi 0g_{9/2} \otimes 2^+_5$	−0.975

transitions induced by the antineutrino scatterings off ^{95}Mo and ^{97}Mo are consistently of the form $\nu 1d_{5/2} \longrightarrow \pi 0g_{9/2} \otimes \omega$.

The reduced one-body transition densities corresponding to the β^- and β^+ transitions between a proton-quasiparticle-phonon state and a neutron-quasiparticle state are given by [22]

$$(p_f\omega_f; j_f \| [c^\dagger_p \tilde{c}_n]_1 \| n_i) = \hat{j_f}\sqrt{3\widehat{J_{\omega_f}}}(-1)^{j_{p_f}+J_{\omega_f}+j_f}\left(\delta_{pp_f}u_p v_n \begin{Bmatrix} j_f & 1 & j_{n_i} \\ j_n & J_{\omega_f} & j_p \end{Bmatrix} \times \sigma^{-1}_{n_i n}\bar{X}^{\omega_f}_{n_i n}(-1)^{j_{n_i}+j_f+1} + \delta_{nn_i}\frac{\delta_{j_f j_p}}{j_f^2} v_p u_n \sigma^{-1}_{p_f p}\bar{Y}^{\omega_f}_{p_f p}\right), \quad (26)$$

and

$$(p_f\omega_f; j_f \| [c^\dagger_n \tilde{c}_p]_1 \| n_i) = \hat{j_f}\sqrt{3\widehat{J_{\omega_f}}}(-1)^{j_p+j_n+j_{p_f}+J_{\omega_f}+j_f}\left(\delta_{pp_f}u_n v_p \begin{Bmatrix} j_f & 1 & j_{n_i} \\ j_n & J_{\omega_f} & j_p \end{Bmatrix} \times \sigma^{-1}_{n_i n}\bar{X}^{\omega_f}_{n_i n}(-1)^{j_{n_i}+j_f+1} + \delta_{nn_i}\frac{\delta_{j_f j_p}}{j_f^2} v_n u_p \sigma^{-1}_{p_f p}\bar{Y}^{\omega_f}_{p_f p}\right), \quad (27)$$

respectively. Moreover, it is well known (see, e.g., Ref. [28]) that the Gamow-Teller operators, $\boldsymbol{\sigma}\tau_\pm$, have nonzero matrix elements only between single-particle states a and b with the same n and l quantum numbers, i.e., one has the selection rules $\Delta l = l_a - l_b = 0$ and $\Delta n = n_a - n_b = 0$. Since the backward-going amplitudes $Y^{\omega_f}_{p_f p}$ are typically small we consider for the present discussion only the terms in Eqs. (26) and (27) which are proportional to $\bar{X}^{\omega_f}_{n_i n}$. Then the QRPA

TABLE IX. QRPA forward amplitudes for some states in ^{94}Mo which are important for the charged-current antineutrino scattering off ^{95}Mo.

Conf	5^+_1	4^+_2	4^+_4	6^+_1	4^+_3	2^+_5
$\nu 1d_{5/2} \otimes \nu 0g_{7/2}$	1.000	0.201	0.938	0.824	−0.160	0.967
$\nu 1d_{5/2} \otimes \nu 0g_{9/2}$	−0.002	0.054	0.025	−0.091	−0.060	0.042

configurations with nonvanishing contributions for the cases $p_f = \pi 1d_{5/2}, \pi 1d_{3/2}, \pi 0g_{9/2}$ are

$$\begin{matrix} \nu 1d_{5/2} \otimes \nu 1d_{5/2} \\ \nu 1d_{5/2} \otimes \nu 1d_{3/2} \end{matrix} ; \quad \text{if} \quad p_f = \pi 1d_{5/2}, \pi 1d_{3/2}, \quad (28)$$

and

$$\begin{matrix} \nu 1d_{5/2} \otimes \nu 0g_{7/2} \\ \nu 1d_{5/2} \otimes \nu 0g_{9/2} \end{matrix} ; \quad \text{if} \quad p_f = \pi 0g_{9/2}. \quad (29)$$

Therefore, we show in Table VIII the QRPA forward-going amplitudes $X^{\omega_f}_{n_i n}$ [see Eq. (15)] for the QRPA configurations given in Eqs. (28) and (29) for some of the phonons which are important for the neutrino scattering off ^{95}Mo, see Table IV. Moreover, in Table IX are tabulated the results for the QRPA phonons which are prominent in the antineutrino scattering (see also Table V). It is seen in the tables that most of the phonons have rather large amplitudes for one or more of the $\nu 1d_{5/2} \otimes \nu 1d_{5/2}$, $\nu 1d_{5/2} \otimes \nu 1d_{3/2}$, $\nu 1d_{5/2} \otimes \nu 0g_{9/2}$, and $\nu 1d_{5/2} \otimes \nu 0g_{7/2}$ configurations. In particular, the importance of the $\nu 1d_{5/2} \otimes \nu 0g_{9/2}$ ($\nu 1d_{5/2} \otimes \nu 0g_{7/2}$) configuration for the neutrino (antineutrino) scattering should be noted.

IV. CONCLUSIONS

In this work we have computed the cross sections for the charged-current neutrino and antineutrino scatterings off the odd-mass $A = 95, 97$ molybdenum isotopes. In the calculations the initial and final nuclear states have been constructed by using the microscopic quasiparticle-phonon model. The nuclear responses to supernova neutrinos for the aforementioned nuclei have been calculated by folding the cross sections with a two-parameter Fermi-Dirac distribution.

Our results show that for both the neutrino and antineutrino reactions the cross sections are dominated by allowed transitions. However, for the anti-neutrino reactions the contributions from the 0^+ multipole are largely suppressed.

TABLE VIII. QRPA forward-going amplitudes for some states in ^{94}Mo which are important for the charged-current neutrino scattering off ^{95}Mo.

Conf	2^+_1	4^+_{10}	6^+_4	5^+_3	2^+_8	4^+_6	2^+_{15}
$\nu 1d_{5/2} \otimes \nu 1d_{5/2}$	−0.631	0.011	–	–	0.003	0.010	−0.018
$\nu 1d_{5/2} \otimes \nu 1d_{3/2}$	−0.227	0.010	–	–	0.022	0.083	0.008
$\nu 1d_{5/2} \otimes \nu 0g_{7/2}$	0.166	−0.029	0.204	0.021	−0.079	−0.082	0.037
$\nu 1d_{5/2} \otimes \nu 0g_{9/2}$	−0.163	0.960	−0.928	0.990	0.034	0.062	−0.864

Consequently, first-forbidden type of transitions mediated by the 1^- and 2^- multipoles become relatively more important.

Furthermore, we have found that for the neutrino scattering off ^{95}Mo (^{97}Mo) leading to final states in ^{95}Tc (^{97}Tc) the most important single-particle transitions transitions are of the forms $\nu 1d_{5/2} \longrightarrow \pi 1d_{5/2}$, $\nu 1d_{5/2} \longrightarrow \pi 1d_{5/2} \otimes \omega$, $\nu 1d_{5/2} \longrightarrow \pi 1d_{3/2} \otimes \omega$, and $\nu 1d_{5/2} \longrightarrow \pi 0g_{9/2} \otimes \omega$ where ω denotes a QRPA (quasiparticle random-phase approximation) phonon. For the antineutrino scatterings to final states in ^{95}Nb and ^{97}Nb the situation is even simpler: the dominant transitions are of the form $\nu 1d_{5/2} \longrightarrow \pi 0g_{9/2} \otimes \omega$.

According our calculations the nuclear responses to supernova neutrinos are not sensitive to whether the neutrino-mass hierarchy is normal or inverted. However, for antineutrinos the cross sections are significantly larger for the normal mass hierarchy than for the inverted hierarchy.

ACKNOWLEDGMENTS

This work has been supported by the Academy of Finland under the Finnish Center of Excellence Program 2012–2017 (Nuclear and Accelerator Based Program at JYFL).

[1] C. Giunti and C. W. Kim, *Fundamentals of Neutrino Physics and Astrophysics* (Oxford University Press, New York, 2007).
[2] D. V. Forero, M. Tòrtola, and J. W. F. Valle, Phys. Rev. D **86**, 073012 (2012).
[3] S. M. Bilenky, C. Giunti, J. A. Grifols, and Massó, Phys. Rep. **379**, 69 (2003).
[4] J. Suhonen and O. Civitarese, Phys. Rep. **300**, 123 (1998).
[5] K. Langanke and G. Martínez-Pinedo, Rev. Mod. Phys. **75**, 819 (2003).
[6] A. B. Balantekin and G. M. Fuller, J. Phys. G: Nucl. Part. Phys. **29**, 2513 (2003).
[7] S. E. Woosley, J. R. Wilson, G. J. Mathews, R. D. Hoffman, and B. S. Meyer, Astrophys. J. **433**, 229 (1994).
[8] A. Heger *et al.*, Phys. Lett. B **606**, 258 (2005).
[9] M.-K. Cheoun, E. Ha, T. Hayakawa, S. Chiba, K. Nakamura, T. Kajino, and G. J. Mathews, Phys. Rev. C **85**, 065807 (2012).
[10] G. G. Raffelt, Prog. Part. Nucl. Phys. **64**, 393 (2010).
[11] H. Ejiri, Phys. Rep. **338**, 265 (2000).
[12] H. Ejiri *et al.*, Eur. Phys. J. Special Topics **162**, 239 (2008).
[13] Helium and Lead Observatory, http://www.snolab.ca/halo/.
[14] LAGUNA-Large Apparatus studying Grand Unification and Neutrino Astrophysics, http://www.laguna-science.eu/.
[15] J. Engel, S. Pittel, and P. Vogel, Phys. Rev. C **50**, 1702 (1994).
[16] E. Ydrefors and J. Suhonen, Adv. High Energy Phys. **2012**, 373946 (2012).
[17] K. Langanke and E. Kolbe, At. Data Nucl. Data Tables **79**, 293 (2001).
[18] B. Dasgupta, A. Dighe, G. G. Raffelt, and A. Y. Smirnov, Phys. Rev. Lett. **103**, 051105 (2009).
[19] J. S. O'Connell, T. W. Donnelly, and J. D. Walecka, Phys. Rev. C **6**, 719 (1972).
[20] E. Ydrefors, K. G. Balasi, T. S. Kosmas, and J. Suhonen, Nucl. Phys. A **896**, 1 (2012).
[21] J.-P. Berrut and L. N. Trefethen, SIAM Rev. **46**, 501 (2004).
[22] J. Toivanen and J. Suhonen, Phys. Rev. C **57**, 1237 (1998).
[23] M. Baranger, Phys. Rev. **120**, 957 (1960).
[24] E. Ydrefors *et al.*, in *Neutrinos: Properties, Reactions, Sources and Detection*, edited by J. P. Greene (Nova Science Publishers, New York, 2011).
[25] J. D. Walecka, *Theoretical Nuclear and Subnuclear Physics* (Imperial College Press, London, 2004).
[26] J. Engel, Phys. Rev. C **57**, 2004 (1998).
[27] E. Kolbe, K. Langanke, G. Martínez-Pinedo, and P. Vogel, J. Phys. G **29**, 2569 (2003).
[28] J. Suhonen, *From Nucleons to Nucleus: Concepts of Microscopic Nuclear Theory* (Springer, Berlin, 2007).
[29] A. Bohr and B. R. Mottelson, *Nuclear Structure*, Vol. I (Benjamin, New York, 1969).
[30] K. Holinde, Phys. Rep. **68**, 121 (1981).
[31] E. Ydrefors, M. T. Mustonen, and J. Suhonen, Nucl. Phys. A **842**, 33 (2010).
[32] G. Martínez-Pinedo, B. Ziebarth, T. Fischer, and K. Langanke, Eur. Phys. J. A **47**, 98 (2011).
[33] J. Gava and C. Volpe, Phys. Rev. D **78**, 083007 (2008).
[34] R. Lazauskas and C. Volpe, Nucl. Phys. A **792**, 219 (2007).
[35] K. Ikeda, Prog. Theor. Phys. **31**, 434 (1964).
[36] M. T. Mustonen and J. Suhonen, Phys. Lett. B **657**, 38 (2007).